JOURNAL OF PROPULSION AND POWER
Vol. 22, No. 5, September–October 2006

Simulation of Void Collapse in an Energetic Material, Part 2: Reactive Case

L. Tran*
Naval Postgraduate School, Monterey, California 93943
and
H. S. Udaykumar†
University of Iowa, Iowa City, Iowa 52242

In Part 1 a numerical methodology was used to study collapse of voids in energetic materials by ignoring the contributions of the gas phase and chemical reaction. In this paper, the thermomechanical response of solid phase is combined with the vapor-phase compression and chemical reactions to study their effects on the energy deposition mechanisms. The formulation and numerical treatment of the coupled solid–gas interactions, including heat release caused by chemical reactions, are discussed. The effects of loading intensity and void size are studied. The results show that for the micron-size voids under consideration significant gas-phase chemical reactions occur. However, their influence on the void collapse itself is minimal. Results indicate that when voids completely collapse a significant amount of reaction products are created, but the collapse time is too short to set up thermal runaway at the hot spot before void collapse.

I. Introduction

WHEN an energetic material is subjected to impact or other loads, ignition can occur at hot spots that typically occur at voids or defects in the material. As a void in an energetic material undergoes elastoviscoplastic deformation under the imposed load, viscoplastic heating and microjetting occur at the void, and the temperature at the material-void boundary attains very high values. The temperature rise can be high enough to cause melting followed by evaporation of the solid material, thereby ejecting gas into the void. To be more descriptive of the situation, the term "solid phase" will be replaced hereafter with "condensed phase" because the solid phase might have undergone solid–solid or solid–liquid transitions under shock loading conditions. Therefore, the material in the vicinity of the void surface is some combination of solid, liquid, and perhaps even gas, all comprising a "foam" layer.[1] In propellant deflagration, for instance, the transition from solid to gas occurs through several layers, that is to say, a solid layer transitions to a liquid or melt layer, which is followed by a foam layer (melt containing gas bubbles). In such a situation the foam layer typically is a few microns in thickness. For the high-pressure detonation situation being studied here, experimental observations indicate that a clear foam layer is not present. Thus, the energetic material appears to transition almost directly from a condensed phase (solid–liquid mixture) to the gas phase.[2]

The typical scenario by which shock loading causes a thermal explosion in an energetic material necessarily involves gas–solid coupling phenomena. The entrapped gas within the void is compressed to high temperature and pressure as the void collapses. The temperature in the gas phase can become high enough to initiate ignition in the gas phase. After the reaction has been initiated in the vicinity of the pores, the condensed surface temperature rises further leading to the propagation of a surface burning wave into the condensed phase. The surface burning in turn deposits gaseous reaction products into the void, which increases the gas pressure. Under suitable conditions, this gas pressure will eventually exceed the condensed-phase pressure and cause a reversal of the plastic flow around the pore, and therefore the void will cease to collapse and can even expand outward.[3] Acceleration of the surface burning wave as a result of gas-phase reactions can generate a secondary compression wave. This compression wave then can interact with the primary shock wave to enhance it. The enhanced wave can impinge on other voids as it propagates from the hot spot and be further strengthened. These mechanisms then combine to result in a runaway explosion of the energetic material.

The scenario just described can be dominant under conditions in which the compression rate is relatively low and the cavities are of the order of a millimeter or larger.[4] For typical void sizes in the micron range, the physics of void collapse remains to be elucidated. Numerical modeling of void collapse and hot-spot formation is a useful means to understand the full range of complex thermomechanical and chemical reaction effects that contribute to energy deposition resulting from shock-void interactions. Previous work in studying void collapse has relied on different levels of complexity, both in terms of treatment of the void collapse as well as the chemical heat-release aspects. The two main works that exemplify analysis of void collapse including chemistry in the gas as well as condensed phases are those by Kang et al.[3] and Conley.[5] In the former the void collapse is assumed to be spherically symmetric, which allows for a one-dimensional treatment of the system and facilitates a semi-analytical approach to solve the equations. In such a geometry the hydrodynamic impact regime described in Part 1[6] cannot be investigated. In the latter work, that is, Conley[5] and Conley and Benson,[7] a mixture formulation is employed, which distinguishes the void region from the rest of the material by means of a condensed-phase fraction variable. A mixture formulation is used to treat the mechanics in those computational elements that are partially occupied by void. Inherent in this treatment are several assumptions regarding the thermomechanical behavior of the "mixed" material. In the present formulation for multimaterial flows, the "mixed" cell treatment is avoided in favor of a sharp-interface treatment. Within this framework the efflux of mass from the condensed phase into the void can be treated without losing information as to the precise location of the void surface. Furthermore, explicit interface conditions between the condensed and gas phases can be applied as in Kang et al.[3] but in a full multidimensional setting.

A further difference between the treatment of Kang et al.[3] and Conley[5] lies in the way in which the mass-transfer rate from the

Received 31 August 2004; revision received 18 November 2005; accepted for publication 18 November 2005.

*Postdoctoral Research Associate, Department of Physics.
†Associate Professor, Department of Mechanical and Industrial Engineering.

condensed to the gas-filled void is modeled. In Kang et al., the mass of condensed material that is converted to gaseous reactants is obtained from a semi-empirical model proposed by Mitani and Williams.[8] The expression used by Kang et al. is

$$m_c^2 = \rho_c k_c T_{c,i} \left\{ \frac{R_u T_{c,i}}{E_c} \right\} \times \frac{A_c \exp[-E_c/(R_u T_{c,i})]}{\{q_c(1-G) - [c_c(T_{c,i}-T_0) - q_c]\,\ell n(1/G)\}} \quad (1)$$

where G is the mass fraction of unreacted vapor entering the pore, q_c the specific heat release in condensed-phase reaction, E_c the activation energy of condensed-phase material, A_c the frequency factor for condensed-phase surface reaction, m_c the mass flux coming from condensed phase, ρ_c the condensed-phase density, k_c the condensed-phase thermal conductivity, $T_{c,i}$ the condensed phase interfacial temperature, R_u the universal gas constant, T_0 the reference temperature, and c_c the condensed-phase specific heat.

This expression was derived based on matched asymptotic expansions[9] assuming a thin reaction zone on the surface of a planar energetic material in the absence of convection in the gas phase and assuming an unstressed and stationary condensed material. It is not clear that these conditions are satisfied in the shock-induced void collapse under investigation in the present work. Therefore, with respect to mass transfer at the interface between condensed and gas phases, an approach similar to Conley was adopted. In this approach all of the gaseous-phase reactants produced at the surface of the condensed phase are assumed to be convected into the void and to subsequently undergo further reactions in the gas phase. The amount of the gaseous-phase reactant produced is obtained based on a chemical kinetics model described next.

II. Kinetics Models for Combustion of HMX

Combustion of nitramines has been studied extensively in the past few decades. A typical combustion pathway involves radical formation, chain branching, recombination, and multibody reactions that occur in hundreds of sequential and/or concurrent steps. Fortunately, most of these steps are quite fast and have negligible thermomechanical effects. The more important reactions steps are ones with longer timescales, and a reduced kinetic model allows treatment of only these rate-controlling steps.

The concept of reduced kinetics models is based on the idea that the prioritization of intermediate reaction steps is inversely related to their reaction rates. Therefore, a complex reaction with hundreds of steps can be represented by a suitable number of slower, rate-limiting reactions. This greatly simplifies a complex reaction to just a few sequential steps.[10,11]

Numerical simulation of void collapse and energy release with detailed chemical models involving over 40 chemical species and 167 chemical reactions was performed by Kang et al.[3] However, in their case the overall numerical complexity is greatly reduced by an assumption of a one-dimensional axisymmetric problem. For multidimensional computations as in the present work, the numerical complexity of taking into consideration all of the detailed chemical reactions becomes prohibitive. Therefore, in this work, as in Bonnett and Butler[12] and Conley,[5] we use a reduced kinetic model proposed by McGuire and Tarver[13] to model the reactions in the condensed and gas phases. We are interested only in how qualitatively distinct species of a reduced kinetics model manifest themselves during hot-spot formation and the subsequent ignition of the reactive material caused by viscoplastic void collapse.

The thermal decomposition of HMX can be modeled as a three-stage process:

$$\underset{C_4H_8N_8O_8}{\text{HMX}} \xrightarrow{1} \underset{CH_2NNO_2}{\text{fragments}} \xrightarrow{2} \underset{CH_2O,N_2O,HCN,HNO_2}{\text{intermediate gases}} \xrightarrow{3} \underset{N_2,H_2O,CO_2,CO}{\text{final gases}}$$

The three major groups of irreversible rate-controlling steps in the HMX decomposition process are 1) unimolecular endothermic breaking of C-N and/or N-N bonds to produce methylene nitramine and other higher molecular weight fragments; 2) weakly exothermic unimolecular decomposition of these condensed-phase fragments to produce intermediate gases: $CH_2O + N_2O$ or $HCN + HNO_2$; and 3) highly exothermic bimolecular gas-phase reactions between these intermediate gases to produce stable reaction products N_2, H_2O, CO_2, CO, etc. Note that of these three mechanisms the first occurs in the condensed phase, and the second occurs at the surface of the condensed phase as well as in the gas phase, whereas the third is a purely gas-phase reaction.

Table 1 Thermal properties of various species[13]

Property	HMX	Fragments	Gases 1	Gases 2
Heat capacity (cal/g-K) at				
293 K	0.24	0.22	0.24	0.27
433 K	0.34	0.31	0.27	0.28
533 K	0.40	0.36	0.29	0.29
623 K	0.46	0.42	0.31	0.30
773 K	0.55	0.50	0.35	0.31
>1273 K	0.55	0.50	0.42	0.35
Thermal conductivity (cal/cm-s-K) at				
293 K	1.23×10^{-3}	6.50×10^{-4}	1.0×10^{-4}	1.0×10^{-4}
433 K	9.70×10^{-4}	5.00×10^{-4}	1.0×10^{-4}	1.0×10^{-4}
533 K	8.10×10^{-4}	4.00×10^{-4}	1.0×10^{-4}	1.0×10^{-4}
>623 K	7.00×10^{-4}	3.00×10^{-4}	1.0×10^{-4}	1.0×10^{-4}
Heat of formation at 298 K (cal/g)	+61.0	+161.0	−139.0	−1339.0

Table 2 Chemical kinetic parameters[13]

HMX $\xrightarrow{1}$	Fragments $\xrightarrow{2}$	Intermediate gases $\xrightarrow{3}$	Final gases
Reaction number	1	2	3
ln frequency factor, s^{-1}	48.7	37.3	28.1
Activation energy, kcal/m	52.7	44.1	34.1
Order of reaction	1	1	2
Heat of reaction at 298 K (cal/g)	+100	−300	−1200

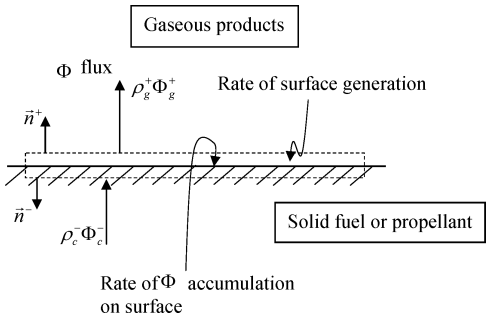

Fig. 1 Illustration of conservation of fluxes at the gas–solid interface.

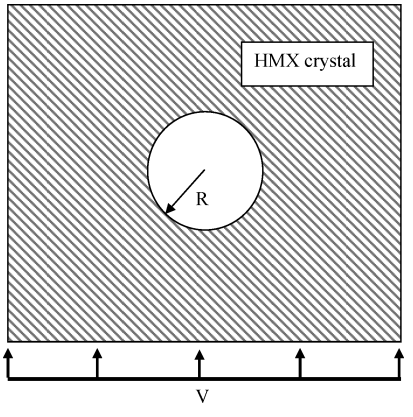

Fig. 2 Schematic of the computational setup for simulation of collapse of a spherical void.

The lumped species for each step are then represented by species A, B, C, and D; therefore, the three reactions are

$$A \rightarrow B \tag{2a}$$

$$B \rightarrow 2C \tag{2b}$$

$$2C \rightarrow D \tag{2c}$$

with thermal and chemical kinetic parameters given in Tables 1 and 2, respectively.

Some comments regarding the preceding decomposition model are in order. First, the preceding model was derived for HMX under conditions corresponding to slow decomposition. Its extension to the present case to situations of surface reaction and shocked flows is, therefore, subject to question. The model carries the virtue of simplicity in terms of the kinetics but should be viewed more as a

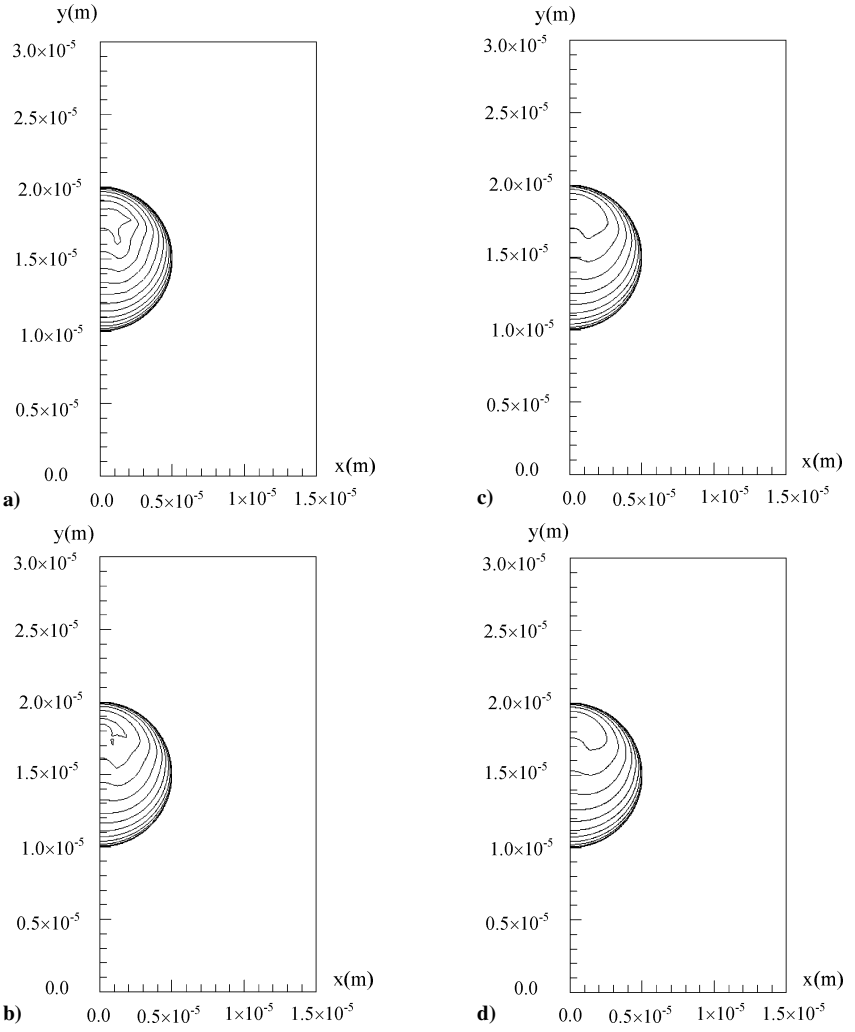

Fig. 3 Void diameter of 10 μm, U_p of 200 m/s, rise time of 10 ns. Evolution of void collapse process is shown for a) 50×100, b) 100×200, c) 150×300, and d) 200×400.

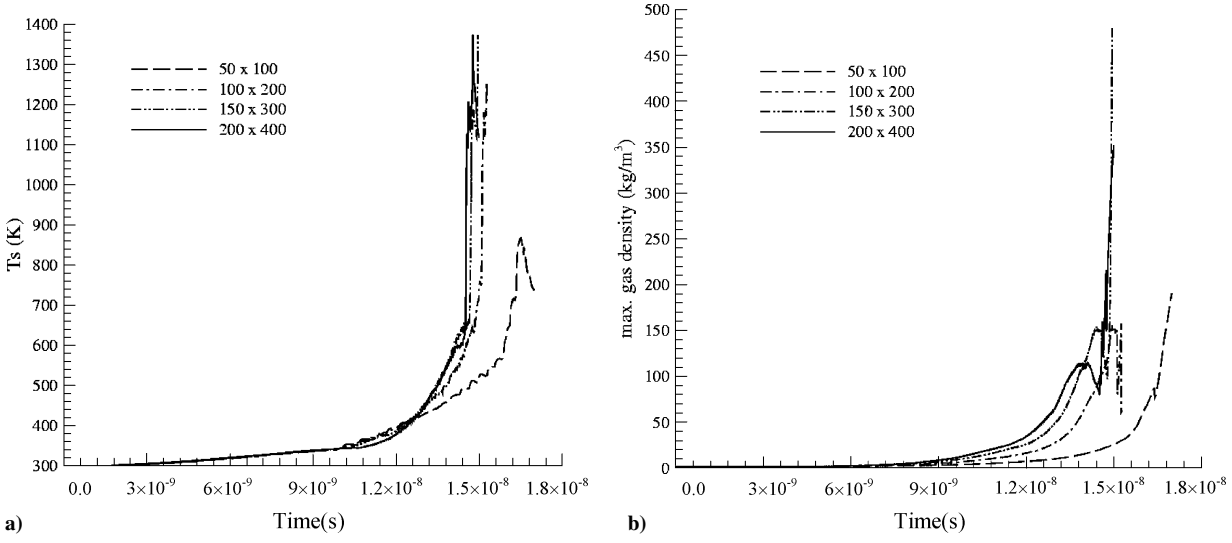

Fig. 4 Grid-independence study for void diameter of 10 μm, U_p of 200 m/s, rise time of 10 ns. Profile of a) maximum solid temperature vs time and b) maximum gas density vs time.

phenomenological model in the context of shock-induced reaction rather than as a true chemical reaction mechanism. In its applied form, as employed by Conley, it allows for the evaluation of the interaction between the energy deposition and localization mechanisms, including inertia, viscoplastic work, void deformation and impact, and the breakdown of HMX as a result of localized heating. As shown in the results, the timescale of collapse of the void is short enough that the reactions listed in the preceding mechanism do not have time to progress to an appreciable extent. Second, in Conley's work there is no clear demarcation between the condensed- and gaseous-phase regions because a mixture formulation is employed. Thus, the preceding three reactions can occur anywhere in the material provided the temperature is high enough to cause significant reaction progress. In the present work, because we avoid the mixture formulation by not having gaseous species within the condensed phase and vice versa, the first reaction occurs only in the condensed phase, the second at the interface between the two phases, and the third only in the gaseous phase. Therefore, we consider only reaction (2a) to occur within the condensed phase. The gasification of species B leads to its transfer into the pore through advection. The gas-phase reactions are then reactions (2b) and (2c).

III. Governing Equations and Numerical Method for Reactive HMX Materials

The governing equations in both gas and condensed phases are solved separately. Under the assumption of a negligibly thin foam zone at the void surface between the condensed and gas phases, gasification is modeled to occur directly from the condensed phase. Similar to the work of Kang et al.,[3] a different set of governing equations is solved in each phase, that is, for the condensed phase and the gas phase within the void. Chemical reaction terms are included in the energy equation. The interface (condensed material-gas) boundary conditions are described in Sec. III.B.

A. Governing Equations

The axisymmetric mass, momentum, and energy conservation equations for each phase are given as follows (with x denoting the radial and y the axial direction):

$$\frac{\partial \boldsymbol{Q}}{\partial t} + \frac{\partial F(\boldsymbol{Q})}{\partial x} + \frac{\partial G(\boldsymbol{Q})}{\partial y} = S(\boldsymbol{Q}) \tag{3}$$

where the vector of conserved variables $\boldsymbol{Q}$ and the convective flux vectors $\boldsymbol{F}(\boldsymbol{Q})$ and $\boldsymbol{G}(\boldsymbol{Q})$ are

$$\boldsymbol{Q} = \begin{Bmatrix} \rho \\ \rho u \\ \rho v \\ \rho E \end{Bmatrix} \quad \boldsymbol{F}(\boldsymbol{Q}) = \begin{Bmatrix} \rho u \\ \rho u^2 + p \\ \rho uv \\ u[\rho E + p] \end{Bmatrix} \quad \boldsymbol{G}(\boldsymbol{Q}) = \begin{Bmatrix} \rho v \\ \rho uv \\ \rho v^2 + p \\ v[\rho E + p] \end{Bmatrix} \tag{4}$$

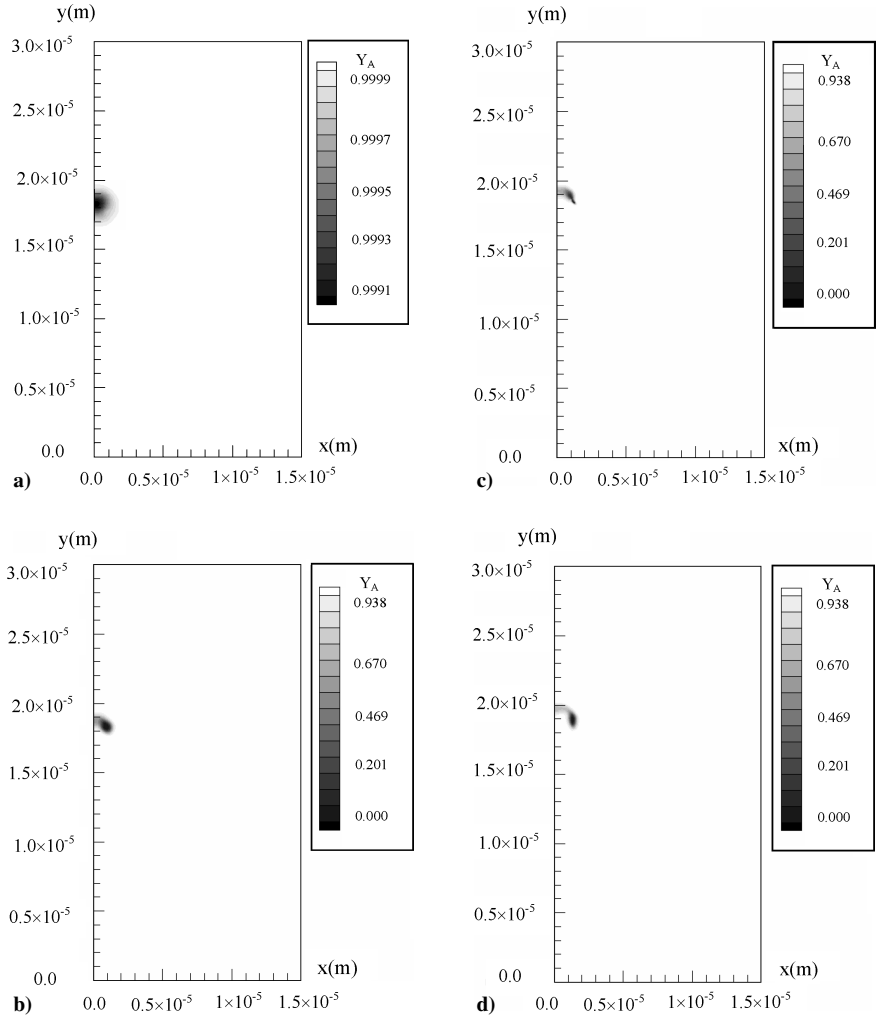

Fig. 5 Void diameter of 10 μm, U_p of 200 m/s, rise time of 10 ns. Species A mass fraction (at the instant of void collapse) for mesh sizes of a) 50×100, b) 100 × 200, c) 150×300, and d) 200×400.

and the vector of source terms is

$$\boldsymbol{S}(\boldsymbol{Q}) =$$

$$\begin{Bmatrix} -\dfrac{\rho u}{x} \\ \dfrac{4}{3}\mu\left[\dfrac{\partial^2 u}{\partial x^2}+\dfrac{1}{x}\dfrac{\partial u}{\partial x}-\dfrac{u}{x^2}\right]+\dfrac{\mu}{3}\left[\dfrac{\partial^2 v}{\partial x\partial y}+\dfrac{1}{x}\dfrac{\partial v}{\partial y}\right]+\mu\dfrac{\partial^2 u}{\partial y^2} \\ \mu\left[\dfrac{\partial^2 v}{\partial x^2}+\dfrac{1}{x}\dfrac{\partial v}{\partial x}-\dfrac{v}{x^2}\right]+\dfrac{\mu}{3}\left[\dfrac{\partial^2 u}{\partial x\partial y}+\dfrac{1}{x}\dfrac{\partial u}{\partial y}\right]+\dfrac{4\mu}{3}\dfrac{\partial^2 v}{\partial y^2} \\ -\dfrac{u(\rho E+p)}{x}+\dfrac{1}{x}\dfrac{\partial}{\partial x}(xus_{xx}+xvs_{xy}) \\ \quad +\dfrac{\partial}{\partial y}(us_{xy}+vs_{yy})+\kappa\left[\dfrac{\partial^2 T}{\partial x^2}+\dfrac{\partial^2 T}{\partial y^2}\right] \\ \quad -\dfrac{\partial}{\partial x}\left(\rho\sum_{i=1}^{N}h_iY_iU_i\right)-\dfrac{\partial}{\partial y}\left(\rho\sum_{i=1}^{N}h_iY_iV_i\right)-\sum_{i=1}^{N}\omega_ih_i \end{Bmatrix} \tag{5}$$

The solid material is treated using a Johnson–Cook model for the constitutive behavior describing the evolution of deviatoric stresses and a Mie–Gruneison equation of state for the pressure. The model includes thermal softening of the material as a result of phase change of the solid. The material parameters for HMX were applied to the solid phase. Details on the mechanical response and its modeling are presented in Sec. I.[6] Note that for the gas phase the deviatoric stresses are given by the viscous stresses with the gas treated as a Newtonian fluid. The fifth and sixth terms in the energy source term are the enthalpy fluxes caused by diffusion velocities of the molecules, whereas the last term represents the energy production caused by chemical decomposition.

A real-gas equation of state, the Noble–Abel equation,[12] is used for the gas phase:

$$p_g = \frac{\rho_g R T_g}{1-\eta\rho_g} \tag{6}$$

where the covolume factor η is 0.001 m^3/kg.

In addition to the preceding system of equations, the species conservation equation is solved in each phase, which is given for the ith species as

$$\frac{\partial}{\partial t}(\rho Y_i)+\frac{\partial}{\partial x}(\rho Y_i u)+\frac{\partial}{\partial y}(\rho Y_i v)=-\frac{\rho Y_i(u+U_i)}{x}$$
$$+\frac{\partial}{\partial x}\left(\rho D\frac{\partial Y_i}{\partial x}\right)+\frac{\partial}{\partial y}\left(\rho D\frac{\partial Y_i}{\partial y}\right)+\omega_i \tag{7}$$

In the preceding system of equations for gas and condensed phases, we assume that the Lewis number $Le=1.0$, that is, $\rho D=\kappa/C_p$. The diffusion velocities are obtained according to Fick's law of mass diffusion:

$$U_i=-\frac{D}{Y_i}\frac{\partial Y_i}{\partial x} \qquad \text{and} \qquad V_i=-\frac{D}{Y_i}\frac{\partial Y_i}{\partial y} \tag{8}$$

The mass production rate for the ith species is determined by the phenomenological chemical kinetic expression, assuming that the reactions are thermodynamically simple:

$$\omega_i = W_i\sum_{k=1}^{M}\left[(\upsilon''_{i,k}-\upsilon'_{i,k})k_f^k\prod_{j=1}^{N}\left(\frac{\rho Y_j}{W_j}\right)^{\upsilon'_{j,k}}\right] \tag{9}$$

where M is the number of reactions, N is the number of species, W_i is the molecular weight of ith species, and $\upsilon'_{i,k}$ and $\upsilon''_{i,k}$ are the stoichiometric coefficients of the reactant and product, respectively.

The reaction rate is based on an Arrhenius form, having unit of s^{-1}:

$$k_f = A\,\exp[-E_a/R_uT] \tag{10}$$

where A is the pre-exponential factor and E_a is the activation energy.

In writing the expression for enthalpy for each species, one has to keep in mind that all species must have the same zero reference

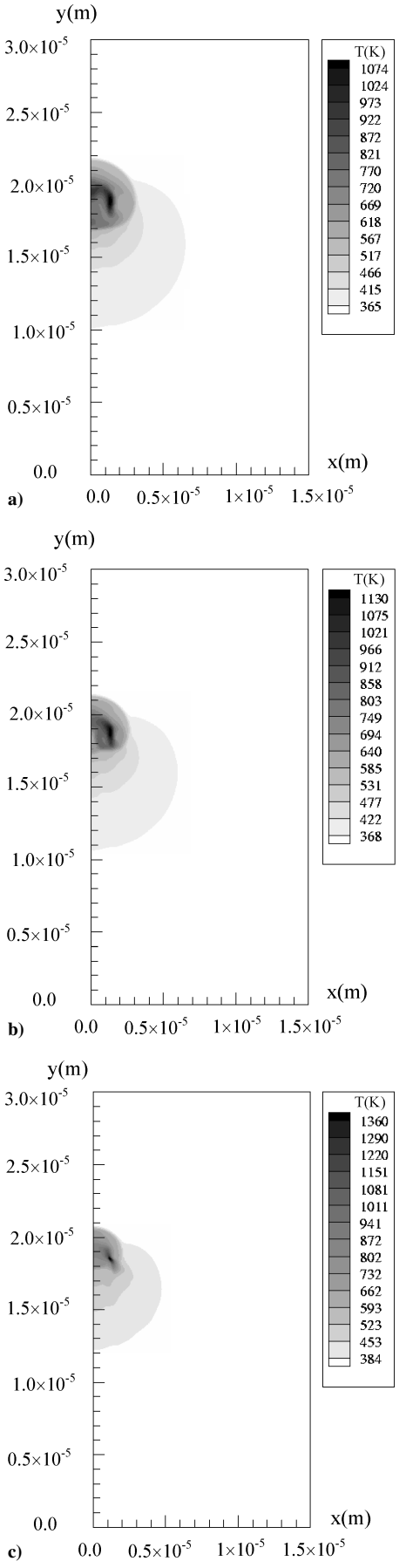

Fig. 6 Void diameter of 10 μm, U_p of 200 m/s, rise time of 10 ns, 150×300 mesh. Temperature contours (at the instant of void collapse) are shown for a) inert, decoupled gas–solid phases; b) inert, coupled gas–solid phases; and c) reactive, coupled gas–solid phases.

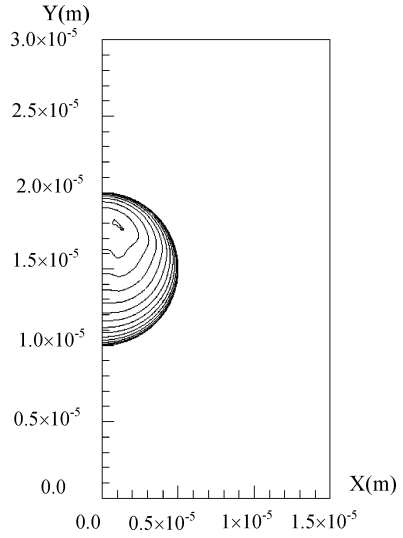

Fig. 7 Evolution of void collapse process for void diameter of 10 μm, U_p of 100 m/s, rise time of 10 ns, and 150 × 300 mesh.

energy level. The expression for enthalpy is then

$$h_i = \Delta h^0_{f,i} + \int_{T_0}^{T} C_{p,i}\, \mathrm{d}T \tag{11}$$

where $\Delta h^0_{f,i}$ is the enthalpy of formation for ith species at reference temperature T_0. Note that, strictly speaking, for the conditions prevailing in the compressible material flow in the solid and gas phases in the simulations presented, and to be consistent with the equation of state, Eq. (6), the enthalpy of the gaseous reactants and products is a function of temperature as well as pressure. Pressure dependency of the enthalpy is not included in Eq. (11) as a simplification. This omission can potentially entail errors in accounting for entropic balances. These errors can occasion instabilities during computations. However, no such instabilities were encountered during the calculations presented in this work, perhaps because the errors are small and overshadowed by physical and numerical dissipative terms in the discretized system of equations.

B. Interfacial Boundary Conditions

The gas-condensed interface boundary conditions can be derived from conservation laws by considering a control volume

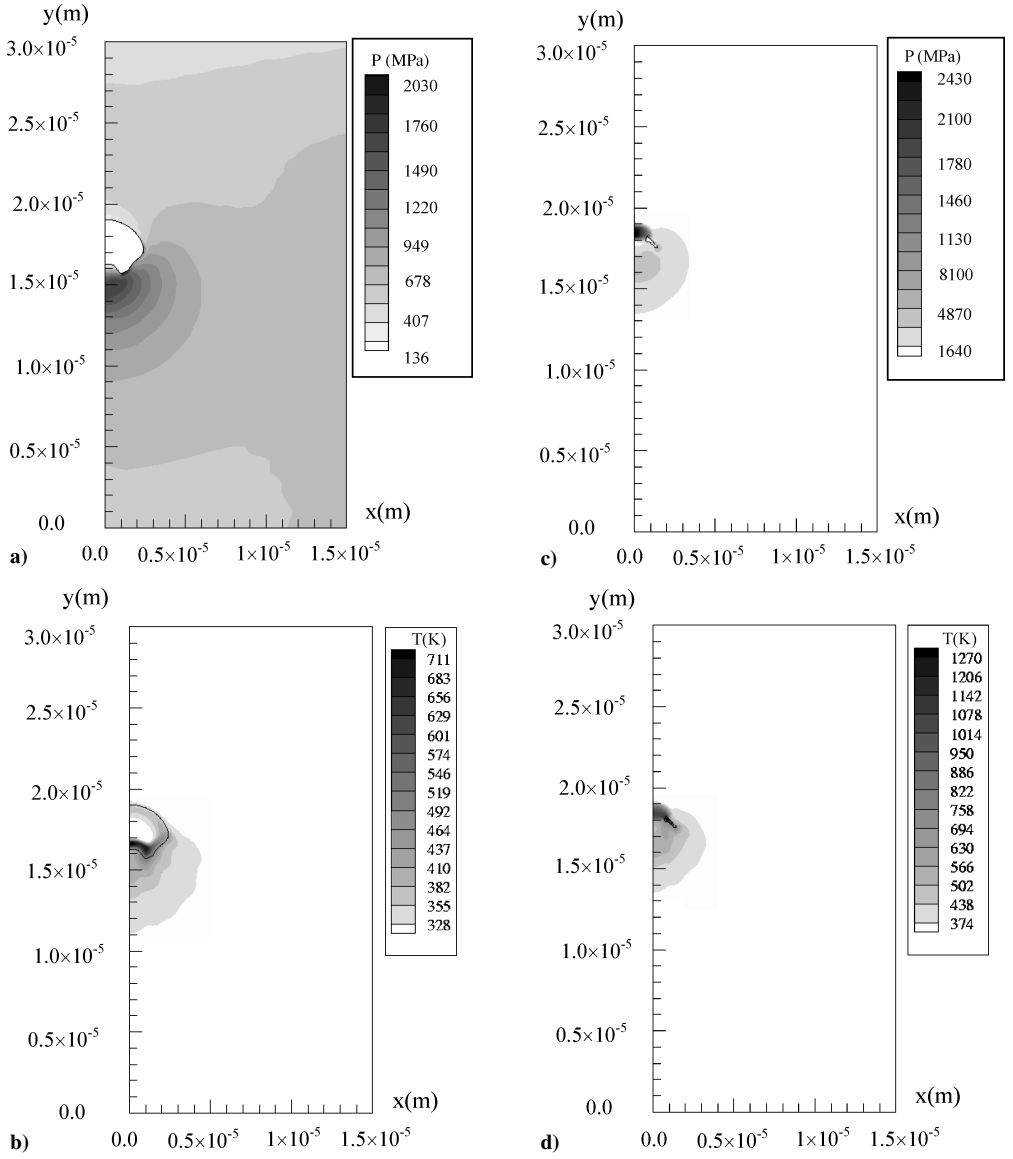

Fig. 8 Void diameter of 10 μm, U_p of 100 m/s, rise time of 10 ns, and 150 × 300 mesh: a) pressure contour at 17 ns, b) temperature contour at 17 ns, c) pressure contour at 18 ns, and d) temperature contour at 18 ns.

surrounding a segment of the interface (Fig. 1). In the limit as the thickness of the control volume approaches zero and assuming there is no mass accumulation within it, the jump conditions for the governing equations are as follows:

Mass conservation:

$$m_c = \rho_c(v_{c,n} - v_{I,n}) = \rho_g(v_{g,n} - v_{I,n}) \tag{12}$$

Momentum conservation:

$$\rho_c U_c(v_{c,n} - v_{I,n}) - \rho_g U_g(v_{g,n} - v_{I,n}) = (\tilde{\sigma}_c - \tilde{\sigma}_g) \cdot \hat{n} \tag{13}$$

where U_c and U_g are respectively velocity vectors in the condensed and gas phases at the interface.

Energy conservation:

$$\rho_c E_c(v_{c,n} - v_{I,n}) - \rho_g E_g(v_{g,n} - v_{I,n}) - \lfloor \tilde{\sigma}_c \cdot \boldsymbol{v}_c - \tilde{\sigma}_g \cdot \boldsymbol{v}_g \rfloor \cdot \hat{n}$$

$$= -(q_{c,n} - q_{g,n}) - \rho_g \sum_{i=1}^{N} Y_{i,g} h_{i,g} V_{i,\mathrm{gn}} + \sum_{i=1}^{N} \omega_i h_i \tag{14}$$

and species conservation:

$$\rho_c Y_{i,c}(v_{c,n} - v_{I,n}) - \rho_g Y_{i,g}(v_{g,n} + V_{i,\mathrm{gn}} - v_{I,n}) = \omega_i \tag{15}$$

where $v_{I,n}$ is the interface velocity along the local normal to the interface, $V_{i,\mathrm{gn}} = V_{i,g} \cdot \hat{n}$ is the mass diffusion velocity along the normal to the interface, and $\tilde{\sigma}$ is the stress tensor. The subscript g denotes gas phase and c denotes condensed phase.

It is easily seen from the preceding jump conditions that there are far more unknowns than available jump conditions. It is therefore necessary to make assumptions regarding the behavior of the fields in the two phases at the interface. For the condensed phase the stresses are treated in a manner similar to that of the inert case. These interface conditions have been described and tested in Tran and Udaykumar.[14] Further, it is assumed that the change in temperature, density, and velocity of the condensed phase in a direction normal to the interface is small compared to the jumps across the interface at the interface. The condensed-phase interface values for these variables are obtained by extrapolation from the interior of the condensed phase.

With the preceding system of jump conditions, extrapolated condensed-phase values, along with the equation of state for the gas phase [Eq. (6)] and the temperature continuity condition at the interface

$$T_I = T_{c,I} = T_{g,I} \tag{16}$$

there are five equations for six unknown interfacial quantities (m_c, $v_{I,n}$, $v_{g,n}$, ρ_g, T_I, p_g).

There are different approaches to resolving this deficiency in the interfacial constraints. The key lies in modeling the mass flux of material from the condensed to the gas phase. If the mass flux was caused by vaporization alone, then the surface temperature and pressure can be linked through thermodynamic relationships. However, in the present problem this mass flux at the interface is caused by a combination of vaporization (condensed-phase species B to

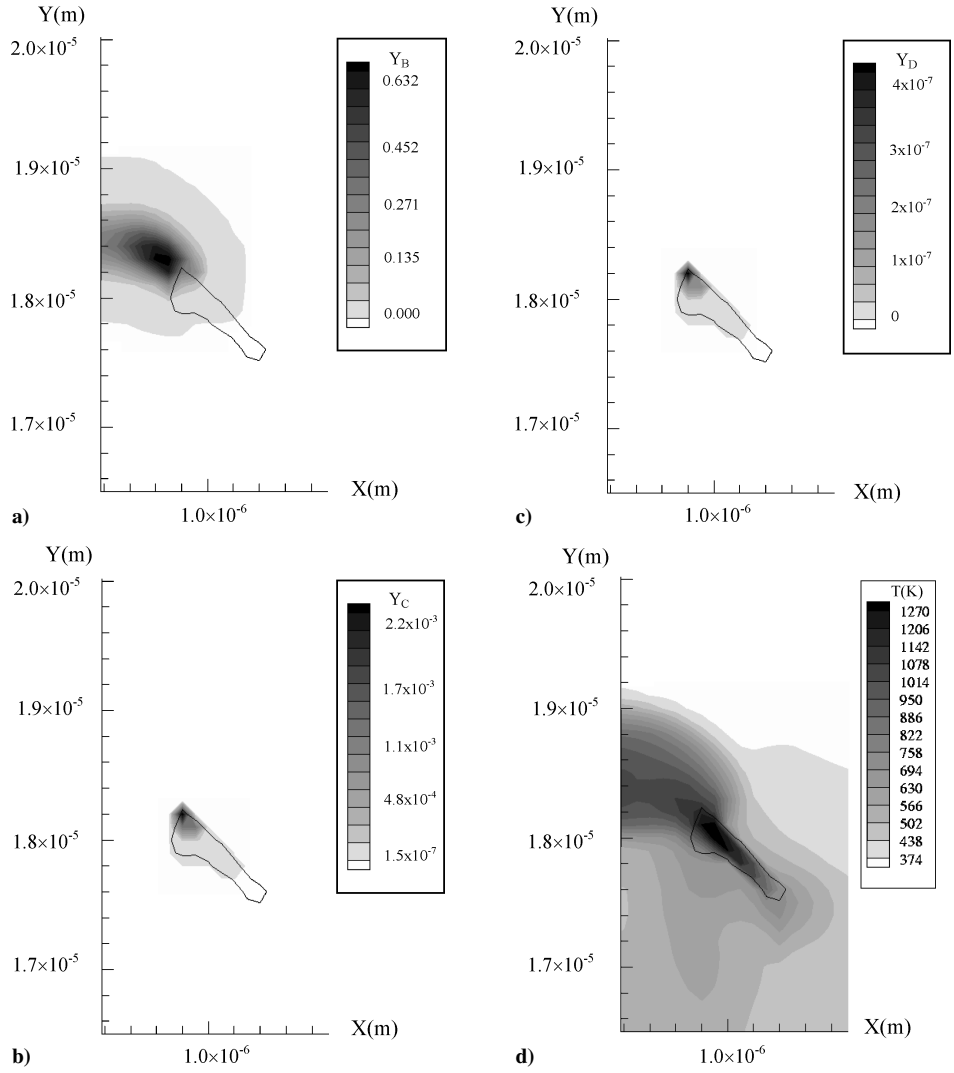

Fig. 9 Void diameter of 10 μm, U_p of 100 m/s, rise time of 10 ns, and 150×300 mesh. Close-up view for a) species B mass fraction contour at 18 ns, b) species C mass fraction contour at 18 ns, c) species D mass fraction contour at 18 ns, and d) temperature contour at 18 ns.

gas-phase species B) and unresolvable subsurface reactions that convert the condensed material (species B) to gas (species C). The fraction of mass transferred from the condensed to the gas phase that can be attributed to vaporization as opposed to chemical reactions is not straightforward to determine. In Kang et al.[3] an approximation to the instantaneous mass flux m_c at the gas-condensed interface [(Eq. (1)] was applied. This semi-empirical approximation, which provides the mass flux as a function of the interface temperature, was obtained through an activation energy asymptotic expansion by Lengelle.[9] In the work of Lengelle, using a matched asymptotic expansion (in the limit of large activation energy) and assuming a steady linear regression, the relationship between surface regression rate and surface temperature is derived. In later studies, of Mitani and Williams[8] and Li et al.,[15] the gas departing the condensed-phase side of the interface was assumed to be composed partly of unreacted vapor enumerated by a factor G (which represents the fraction of unreacted vapor-phase energetic material) and partly of products of an exothermic surface reaction. The curve fits for G to the experimental results of Mitani and Williams,[8] obtained by Kang et al.,[3] show that the mass fraction of unreacted vapor is a weak function of interface temperature.

Using activation energy asymptotic solutions for steady-state deflagration waves, Mitani and Williams[8] were able to obtain an expression for the regression rate as a function of surface temperature under certain restrictive assumptions. Briefly, the assumptions involved in obtaining the instantaneous mass flux at the gas-condensed interface were steady-state deflagration, steady regression of the propellant surface, low pressure (compared to material yield strength), and to a certain extent the material properties did not change appreciably from the bulk unreacted material. In our analysis of inert HMX material under high-pressure shock loading (Part 1[6]), we have found that large gradients exist around the collapsing pores, the behavior of the material is highly nonlinear, and thus many of the limiting conditions underlying the Mitani and Williams approach are violated. Furthermore, the size of the void [$\mathcal{O}(\mu)$] is such that the subsurface reaction zones [also of $\mathcal{O}(\mu)$] can no longer be considered to be asymptotically thin regions. The extent of the softened, partially liquid condensed-phase region at the collapsing void cannot be neglected when compared to the void radius.

Therefore, because of the preceding reasons, we chose not to apply the closed-form expression for interface mass flux to close our system of interfacial boundary conditions. Instead, we have followed, in part, the approach taken by Conley.[5] In Conley's work, the density, energy, and species are diffused across the interface using a mixture formulation. Through this treatment, the mass flux, which accounts for unreacted vapor entering the pore, is handled naturally by assuming that the flow of material across the interface is caused by advection of the material at the speed of the local front. Therefore, as far as the treatment of the species concentrations at the interface is concerned the condensed and gas materials are treated as continuous. Because of this treatment, whatever gas species is produced at the computational nodes in the condensed phase that lie adjacent to the void surface is directly advected into the gas phase in the void. The interface temperature is taken as continuous at the interface between the gas and condensed phases. Finally, the stress boundary condition is satisfied through Eq. (13), once the interface

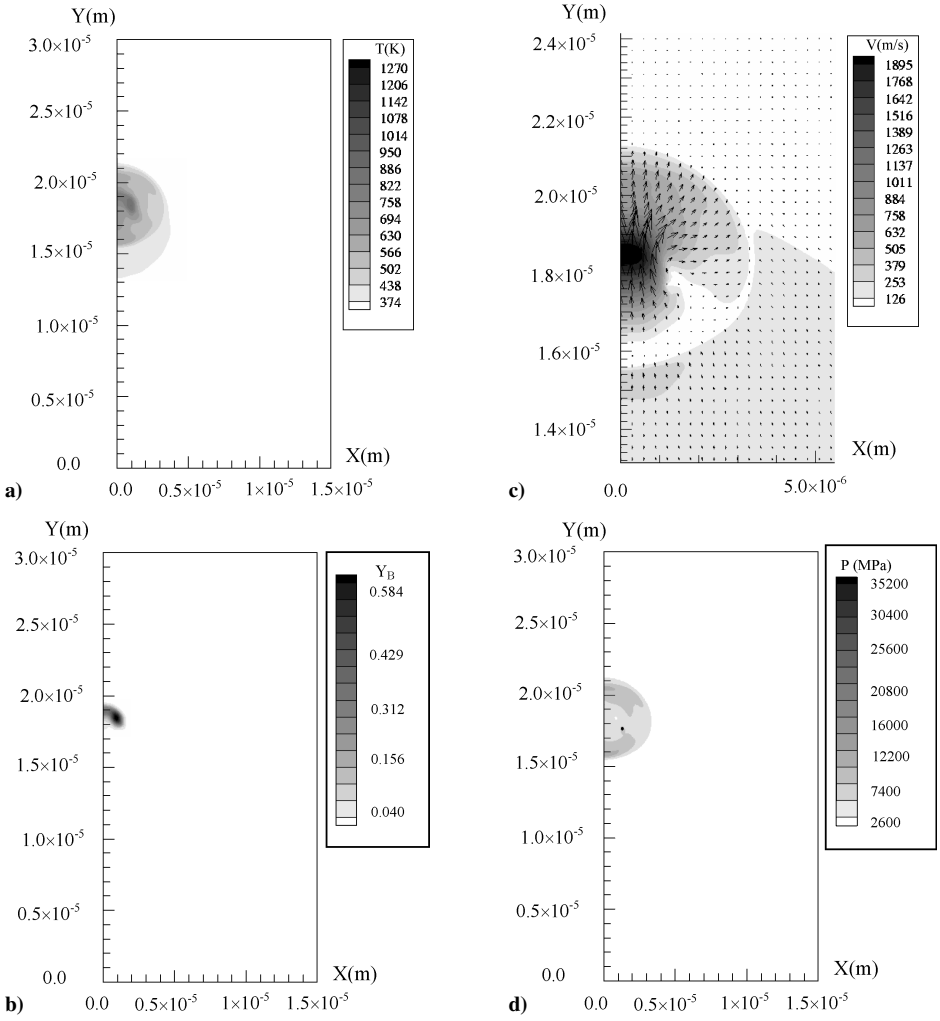

Fig. 10 Void diameter of 10 μm, U_p of 100 m/s, rise time of 10 ns, and 150×300 mesh. At instant of void collapse (18.4 ns), shown are a) temperature contour, b) species B mass fraction contour, c) velocity magnitude contour along with velocity vector, and d) pressure contour.

velocity is determined and the gas-phase pressure is obtained using the approach given in Tran and Udaykumar.[14]

C. Initial Conditions and Reference State

The initial conditions specify an equilibrium state between the gas phase and condensed phase. The void is initially considered to be completely filled with inert gas. Although this inert gas takes on the physical properties of the final gas products, it is energetically insignificant and does not have a role in determining enthalpy fluxes in our calculations.

Therefore, at $t = 0$,

$$T_c = T_g = T_0 \tag{17}$$

In the condensed phase:

$$Y_A = 1.0, \qquad Y_B = Y_C = Y_D = Y_{\text{Inert}} = 0.0 \tag{18}$$

In the gas phase:

$$Y_{\text{Inert}} = 1.0, \qquad Y_A = Y_B = Y_C = Y_D = 0.0 \tag{19a}$$

$$p_g = p_0 \tag{19b}$$

$$\rho_g = \rho_{g,0} \tag{19c}$$

The subscript 0 denotes the reference state with values: $T_0 = 298$ K, $p_0 = 1.0$ atm, and $\rho_{0,g} = 1.38$ kg/m^3. The melting temperature at reference conditions is 558 K with condensed phase shear modulus of 12.0 GPa.

D. Numerical Method for Stiff System of Equations

Because of the fast reaction rates as temperatures increase (Table 2), the timescales for chemical reactions and for the flow can become different by orders of magnitude. During a flow time step Δt, which satisfies the Courant stability condition for the flow, chemical species production rates can be high enough to lead to large excursions in temperature, pressure, and density during that time interval. Therefore, naïve treatment of the preceding system of equations can lead to numerical instability. To circumvent this, severe constraints on computational time steps might need to be placed rendering the flow calculations infeasible. One way to overcome this classic stiffness problem is to advance the entire system of equations for the flow dynamics and chemical reactions in a time-implicit fashion. This approach calls for inversion of large matrix systems leading to time-intensive computations. An alternative is to resort to Strang operator splitting[16] of the governing equations. In this approach, in the first step the flow calculations are performed using the usual explicit approach governed by the Courant–Friedrichs–Lewy time-step constraint without inclusion of the chemical reaction source terms. In the next step, the time stepping is treated implicitly by including the source terms alone. For example, a general evolution equation for a variable Q can be considered where the right-hand side is composed of two parts, the first consisting of all transport terms and the second the chemical reaction contributions:

$$\frac{\mathrm{D}Q}{\mathrm{D}t} = S^I + S^R \tag{20}$$

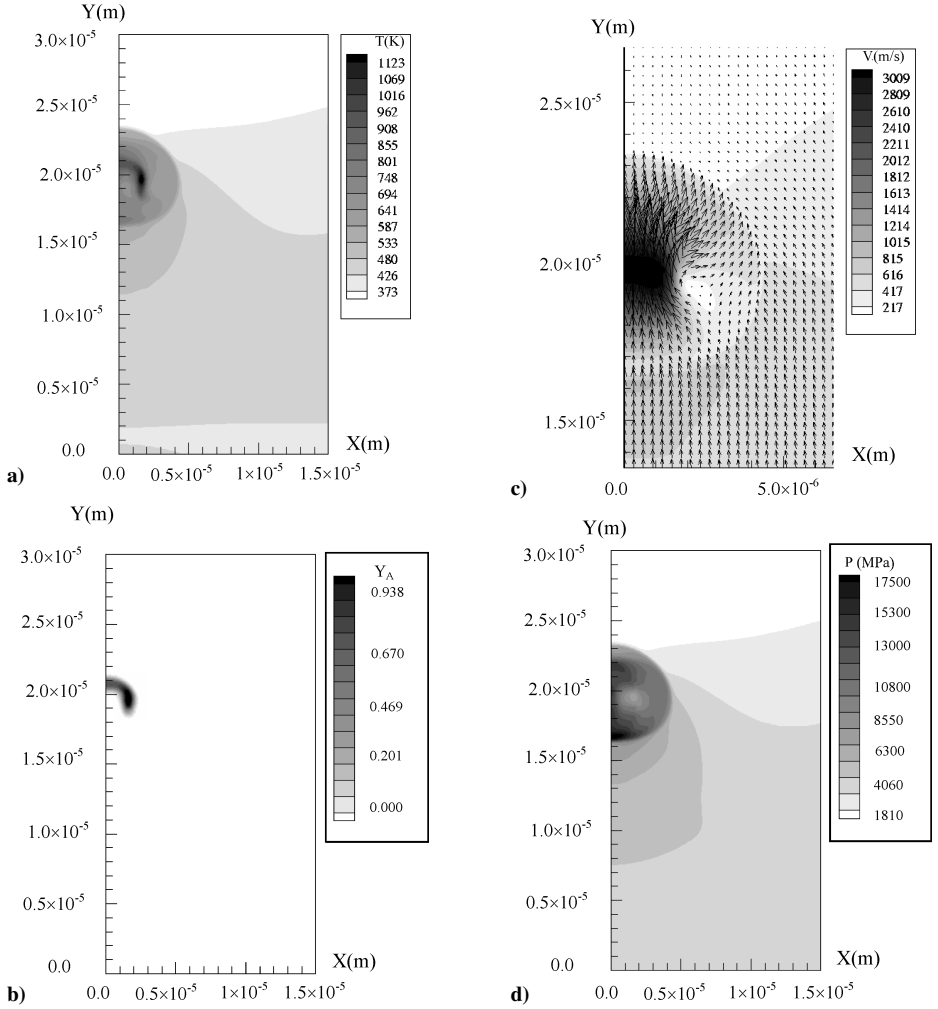

Fig. 11 Void diameter of 10 μm, U_p of 500 m/s, time rise of 10 ns, and 150×300 mesh. At instant of void collapse (11.9 ns), shown are a) temperature contour, b) species B mass fraction contour, c) velocity magnitude contour along with velocity vector, and d) pressure contour.

We solve the system of equations with transport terms using the already described numerical method.[13]

$$\frac{\mathrm{D}Q^*}{\mathrm{D}t} = S^I(Q^n) \tag{21}$$

Then, to obtain the new solution at time level $(n+1)$, we apply a backward Euler implicit scheme to treat the stiff chemical source term:

$$\frac{\mathrm{D}Q^{n+1}}{\mathrm{D}t} = S^R(Q^{n+1}) \tag{22}$$

This numerical treatment provides for stable computations in the presence of stiff source terms; however, it is only first-order time accurate. Also, the stability of the time-split approach can be unreliable for some systems where the stiff source terms are confined to very thin reaction zones that cannot be captured by reasonable mesh sizes.[17]

IV. Results

The setup for all calculations performed in this section is as shown in Fig. 2, assuming a two-dimensional axisymmetric problem. A shock-loading condition is applied at the bottom boundary by imposing a particle velocity at the bottom domain boundary as described in Sec. I.[6] In the present case, the resulting shock profile has a finite, linear rise time, and once it reaches the desired peak shock pressure it attains a constant particle velocity and therefore a steady compressive loading condition.

In the following, a grid-independence study is performed to establish a suitable mesh density for the subsequent calculations. Next, in order to assess the relative importance of the different phenomena that lead to energy localization a comparison is carried out for the solid-phase and gas-phase thermal characteristics for void collapse in three cases, which is to say: 1) inert-decoupled (ID) case where the gas-phase reactions are switched off and the effect of pressure rise of the gas is not transmitted to the condensed phase thereby effectively decoupling the two phases; 2) inert-coupled case (IC) where the reactions are turned off but the gas-phase pressure is transmitted to the condensed phase in the interfacial momentum balance; and 3) reactive-coupled case (RC) where reactions are allowed to occur in the gas in addition to coupling of the gas and solid phases.

The purpose of studying these three cases is to isolate the effects of gas–solid mechanical coupling and chemical reactions in the energy localization process. In Sec. IV.C, the effect of shock-loading strength on the behavior of void collapse process is investigated for two different void diameters. Finally, the effect of shock rise time for a void with diameter of 10 μm and a loading velocity of 200 m/s is studied. This issue is important considering various rise times, and void collapse times are reported in literature. For example, in Kang et al.[3] the rise time was on the order of tenths of a microsecond, whereas in Conley's work[5] the rise time was on the order of tens of nanoseconds. For the loading conditions considered here the typical void collapse timescale is of order of tens of nanoseconds. Although there are other fundamental differences between these two works as discussed in preceding sections, a clear delineation of rise-time effects would be useful to understand not only the results of the present work but also to enable comparison with those of Kang et al.[3] and Conley.[5] Therefore the sensitivity of the results to shock rise time is examined.

A. Grid-Independence Study

To establish the framework for further calculations, grid independence of solutions is assessed for a typical test case with void diameter of 10 μm, loading velocity of 200 m/s, and a shock rise time of 10 ns. Four mesh sizes considered are 50×100, 100×200, 150×300, and 200×400. The evolution of the pore collapse process is shown in Figs. 3a–3d. It is clear that the modes and rates of void collapse for the coarser meshes are somewhat different from that for the finest mesh. However the solutions for the 150×300 and 200×400 meshes show convergence. The effect of grid size on the temperature field produced by the void collapse is shown in Fig. 4a. As seen in the figures, the maximum temperatures achieved are higher for the finer mesh concentration. The localization of the high-temperature zones is also high for the finer meshes. For the maximum value of the gas density in the pore, shown in Fig. 4b, there is still a noticeable difference between the 100×200 and 150×300 meshes. This shows the gas-phase solution is more sensitive to mesh size than the condensed-phase solution. This is perhaps because of the higher compressibility of the gas and hence the formation of higher gradients of the flow variables in the gas phase. These larger gradients demand finer meshes to obtain accurate results. Furthermore, there is some anomalous behavior of the gas density, that is, the solution does not appear to converge monotonically for the finer meshes. This is because the recorded value of the gas density might be high in local spots trapped in small underresolved voids that form when the overall large void collapses and pinches into small pockets that subsequently vanish. It is computationally infeasible to fully resolve the behavior of the complex interfaces and flowfields down to the smallest pores that form in the final stages of void collapse. The impact of the differences in the void shapes during collapse can be significant for the chemical species calculations as shown in the mass fraction contours of species A in Figs. 5a–5d, respectively. These figures show the concentration contours of A plotted at the time when the pore has collapsed completely. For the underresolved mesh (50×100), the mass fraction contours are completely inaccurate, with almost no conversion to species B. For the 200×400 mesh, a grid-independent solution can be considered to have been reached. However, at the instants of void collapse,

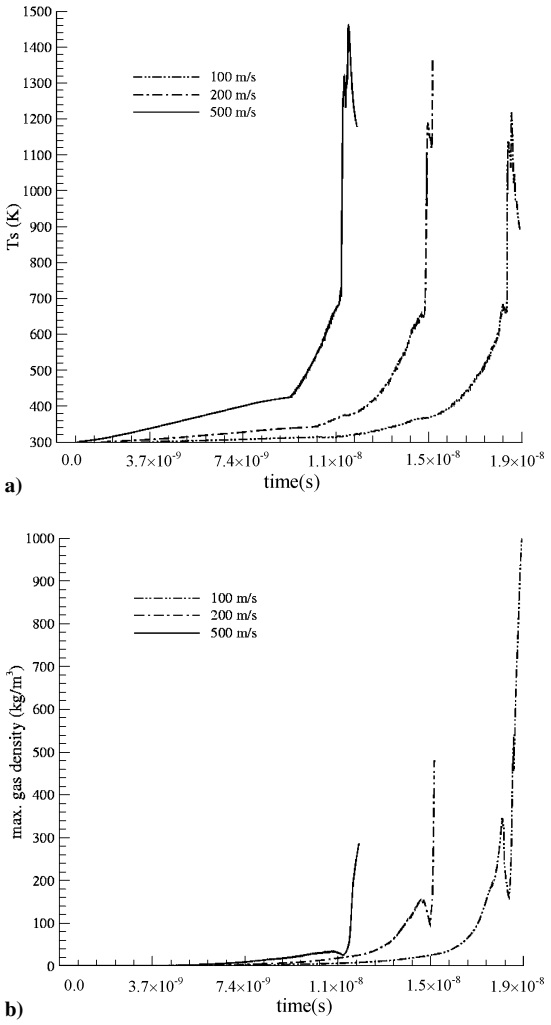

Fig. 12 Effect of loading velocities for void diameter of 10 μm, rise time of 10 ns, and 150×300 mesh. Profiles of a) maximum solid temperature vs time and b) maximum gas density vs time.

that is, when the gas pockets have shrunk to occupy dimensions of the order of the mesh size, the solutions obtained in the gas phase cannot be considered to be accurate. Significant grid effects and numerical dissipation caused by the local smoothing provided by the essentially nonoscillatory scheme will pollute the solution at such instants. This limitation exists in the present as well as other numerical solutions of formation of singularities, such as in the collapse of voids.

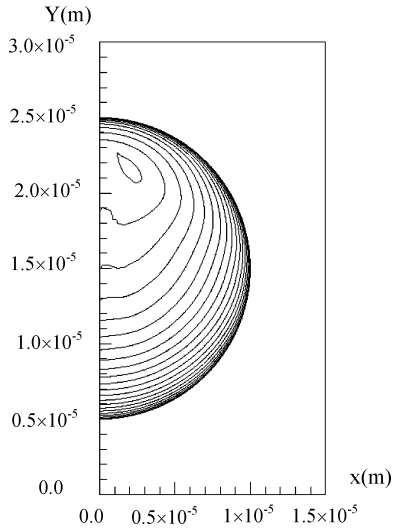

Fig. 13 Evolution of void collapse process for void diameter of 20 μm, U_p of 100 m/s, rise time of 10 ns, and 150 × 300 mesh.

B. Effects of Gas–Solid Coupling and of Reactions in the Gas Phase

Calculations were carried out for the ID, IC, and RC cases (described in Sec. IV) for a test case with void diameter of 10 μm, loading velocity of 200 m/s, rise time of 10 ns, and a mesh size of 150 × 300. The objective is to examine whether and how the gas-phase affects the behavior of the void collapse process for inert and reactive calculations. All of the figures shown in this section are plotted at the time instant when the void has collapsed completely. These time instants are only slightly different for each test case: 15.8 ns for inert decoupled, 15.6 ns for inert coupled, and 15.0 ns for reactive coupled. This indicates that the collapse is mainly driven by the effect of the incident shock and that compression of the gas phase has only a minimal effect on the void collapse timescale for the case already examined.

Figures 6a–6c show the contours of temperature for ID, IC, and RC cases. The temperature rise for the ID and IC cases are not high enough to have significant condensed-phase reaction from species A to species B even after complete collapse of the void. From the temperature contours, it is clear that the maximum temperature area is localized and smoothly varies away from the maximum values. Note the higher temperatures reached in the case where the reactions are present in the gas (the RC) case when compared to the IC case. There are only small differences in the temperature contours between ID and IC cases while for the RC case the higher temperature rise is localized more than for the inert cases. Overall, these calculations indicate that the mechanical coupling between the gas phase and condensed phase is weak, which is to be expected because the gas pressure through the entire void collapse process is a few orders of magnitude below the condensed-phase pressure. For the void size, shock strength, and rise time considered, there is insufficient

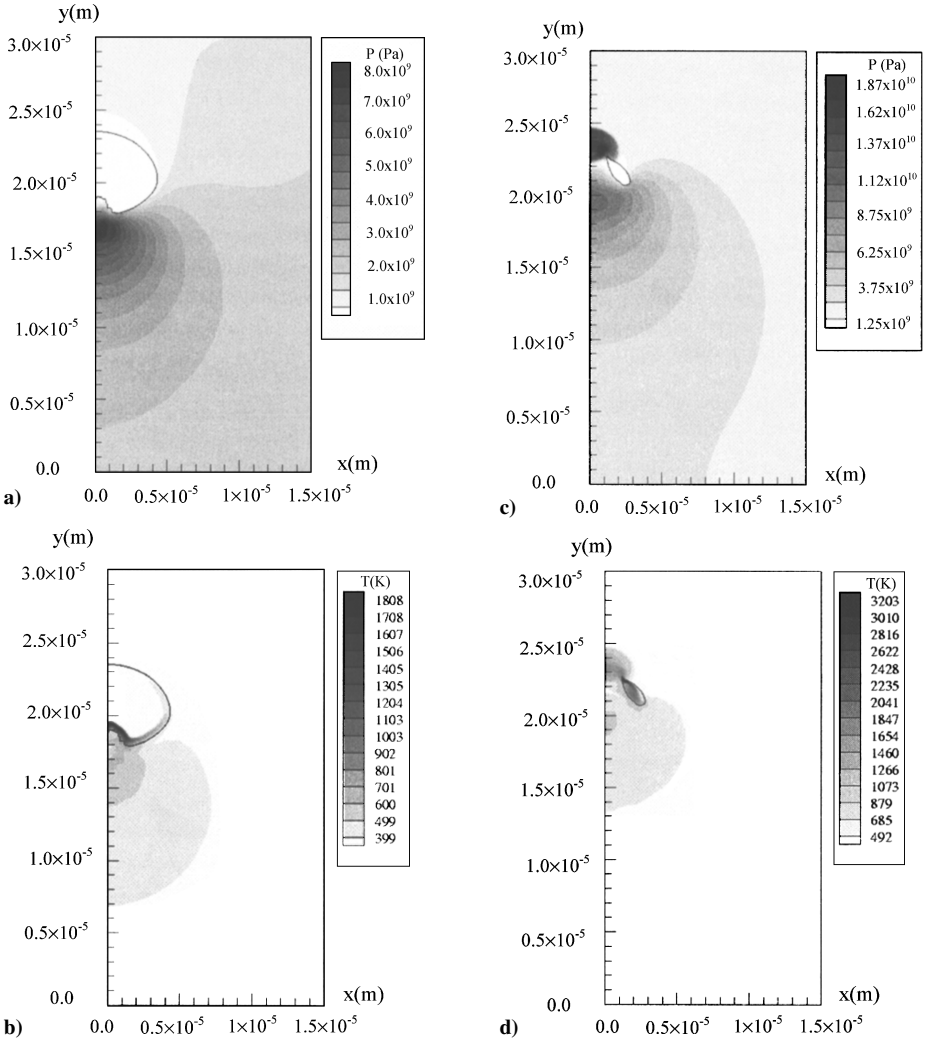

Fig. 14 Void diameter of 20 μm, U_p of 100 m/s, rise time of 10 ns, and 150 × 300 mesh. Shown are contours of a) pressure at 23 ns, b) temperature at 23 ns, c) pressure at 24 ns, and d) temperature at 24 ns.

time for the gas in the void to be compressed to high pressures before the void completely collapses. As it turns out from calculations that will be covered later in this chapter, there is insufficient conversion of the condensed-phase material into the gaseous phase for the parameters chosen for this test case. Therefore there is negligible gas-phase energy release, and the gas pressure in the void does not achieve the high values reported in Kang et al.,[3] where larger voids were considered.

C. Effects of Loading Conditions

Next the behavior of the void and the energy release in the hot spot is studied for different loading conditions for two void diameters, 10 and 20 μm. The particle velocities for the bottom boundary considered are 100, 200, and 500 m/s with a mesh size of 200×400 to ensure grid-independent solutions. The rise time for all test cases is 10 ns.

1. Void Diameter of 10 μm

The void collapses in this case in about 18.4 ns. The mode of collapse in shown in Fig. 7 plotted at equal intervals of time. The formation of a weak jet in the lower part of the void and the pinching of the void to form disconnected pockets is seen in the figure. Figures 8a–8d show the contours of pressure and temperature at two times during the collapse of the void, that is, 17 and 18 ns. The condensed-phase pressure is three orders of magnitude higher than the gas-phase pressure; hence, even though the void contains gas under pressure, the contours of pressure do not show up significantly in the void. At $t = 17$ ns (Fig. 8b) the condensed-phase temperature is still low, around 400–500 K, and the temperature rise is exclusively caused by viscoplastic work being dissipated into heat. The gas temperature shows the highest values in the domain, and the high temperatures are concentrated around a thin region where the interface deforms the most. The compression of the gas in this region is very high. The large temperature gradients in the gas show that conduction effects in the gas phase are insignificant. In fact, the timescales for thermal diffusion in the gas phase are much longer than the timescale for collapse considered here. Note that radiation has been neglected in the current work as a means of transmission of energy from the gas phase to the solid phase; therefore, apart from convection there is no other effective mechanism for heat transfer between the gas and condensed phase. The rise in temperature observed in Fig. 8b is caused purely by gas-phase compression because there is no reaction occurring in the pore at the instants shown. This is because the condensed-phase temperature has not reached a value high enough to cause a significant breakdown of species A to B (typically temperatures of 800 K or higher are required for gaseous reactants to fill the void) and for the subsequent breakdown of B into the gaseous reactants. At around 18 ns, the jetting of lower void surface occurs, the jet impacts with the upper surface, and the void collapses completely (Figs. 8c and 8d). The pressure resulting from this hydrodynamic impact is an order of magnitude higher than the value before impact (compare Fig. 8c to Fig. 8a). There is also a rise in temperature in a localized region corresponding to the jet impact location as seen in Fig. 8d.

To obtain a better picture of the behavior near the point where the void has pinched to give a disconnected pocket of gas, a closer view of the region near the pocket of gas is plotted in Fig. 9. As can be seen in Fig. 9a, the high-temperature region at the point of

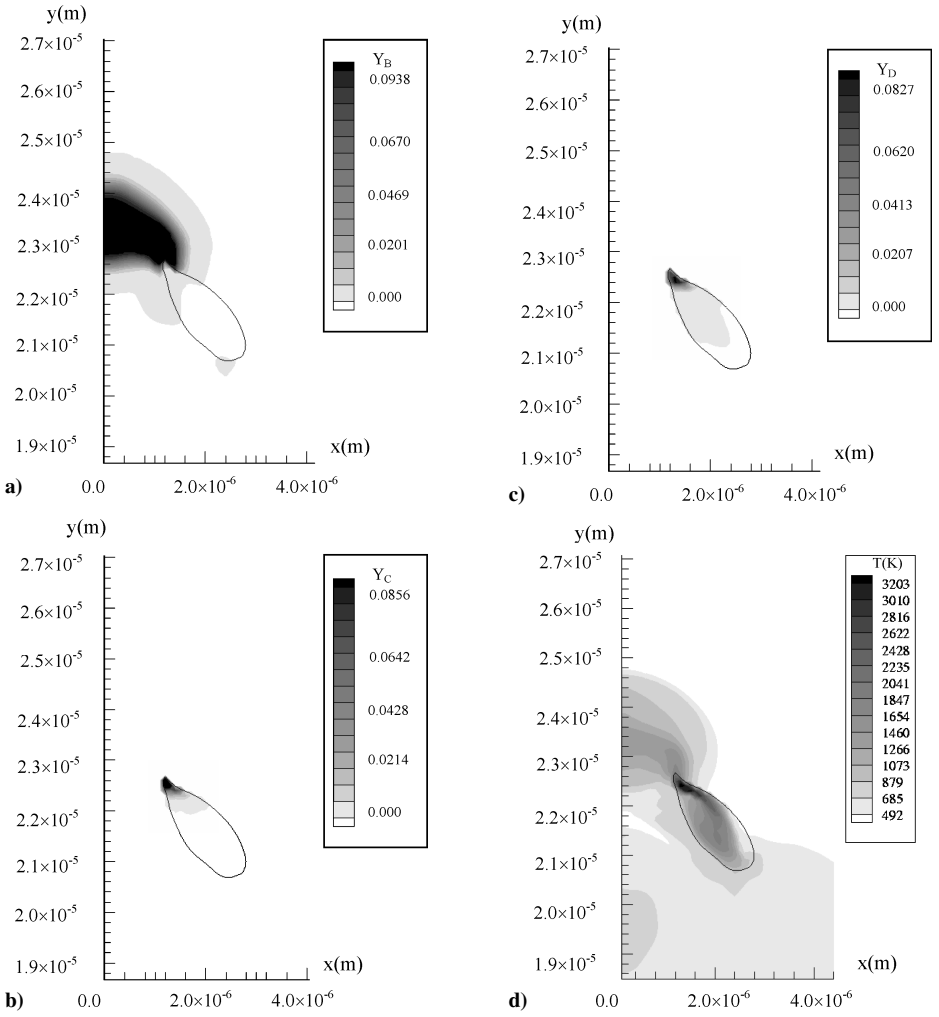

Fig. 15 Void diameter of 20 μm, U_p of 100 m/s, rise time of 10 ns, and 150×300 mesh. Shown are close-up view of contours at 24 ns of a) species B mass fraction, b) species C mass fraction, c) species D mass fraction, and d) temperature.

impact leads to breakdown of species A into B. Furthermore, there are further gas-phase reactions that occur in the high-temperature region adjacent to the point where the jet impacts. This results in some production of the gas-phase species C (Fig. 9b) and of species D (Fig. 9c). These gas-phase reactions are exothermic and lead to a high-temperature region (Fig. 9d) in the gas trapped in the pocket that is left after the jet has impacted with the top surface of the void. At 18.4 ns the remaining gas pocket has also collapsed, and in this case the temperature (Fig. 10a) of the remaining material is not very high. The amount of B species produced (Fig. 10b) after the void has entirely collapsed is also minimal. Following void collapse the velocity of the material (Fig. 10c) in the vicinity of the collapse is extremely high. As shown in Fig. 10d, a nearly spherical compression wave emanates from the location of the void collapse and propagates into the surrounding condensed phase.

The important insight obtained from the preceding case is that, for the parameters investigated, chemical reaction is not significant prior to void collapse. This is because the temperatures are not high enough to induce the transformation from A to B species, that is, for the breakdown of the polymer to occur. Consequently the reactions that follow, that is, from B to C and thereafter to D, do not occur to any significant extent for this low-velocity case.

For a high loading velocity of 500 m/s, similar observations can be made as for the two preceding 100-m/s cases. Obviously, as the impact velocity is increased the phenomena noted in the previous two cases become more severe. The jet impact is stronger, and the production of species B is more noticeable. However, even for this high-velocity case, the viscoplastic heating raises the condensed temperature to about 600 K, which is still too low for significant $A \rightarrow B$ reaction to take place in the condensed phase. When the void has completely collapsed (at a time of 11.9 ns), the temperature (Fig. 11a), species B (Fig. 11b), particle velocities (Fig. 11c), and pressure (Fig. 11d) all show higher intensities than for the previous low-velocity cases. A strong, nearly spherical shock wave emerges from the collapsed void. There is a significant focusing effect during void collapse, and the particle velocities (Fig. 11c) at the point of collapse are nearly six times that of the imposed far-field particle velocity of 500 m/s.

The question remains as to why in all of these cases we do not observe significant chemical reactions occurring prior to void collapse? There are several reasons for the lack of runaway reactions. The void collapse occurs very quickly. The viscoplastic work does not heat the solid material to high enough temperatures to break down the polymer (A) to monomers (B). Thus there is insufficient B species advecting into the gas. The breakdown process $A \rightarrow B$ is endothermic. Therefore when this reaction occurs it actually lowers the condensed-phase temperature further hindering the formation of species B. Whatever B has been advected into the void can undergo further gas-phase reactions to form C and D. These exothermic reactions could then raise the temperature of the gas leading to a thermal feedback to enhance the reactions. However, because the void collapses very quickly there is little time for the exothermic reactions to progress enough to have a significant impact. The gas-phase density and pressures have not built up enough to prevent the void from

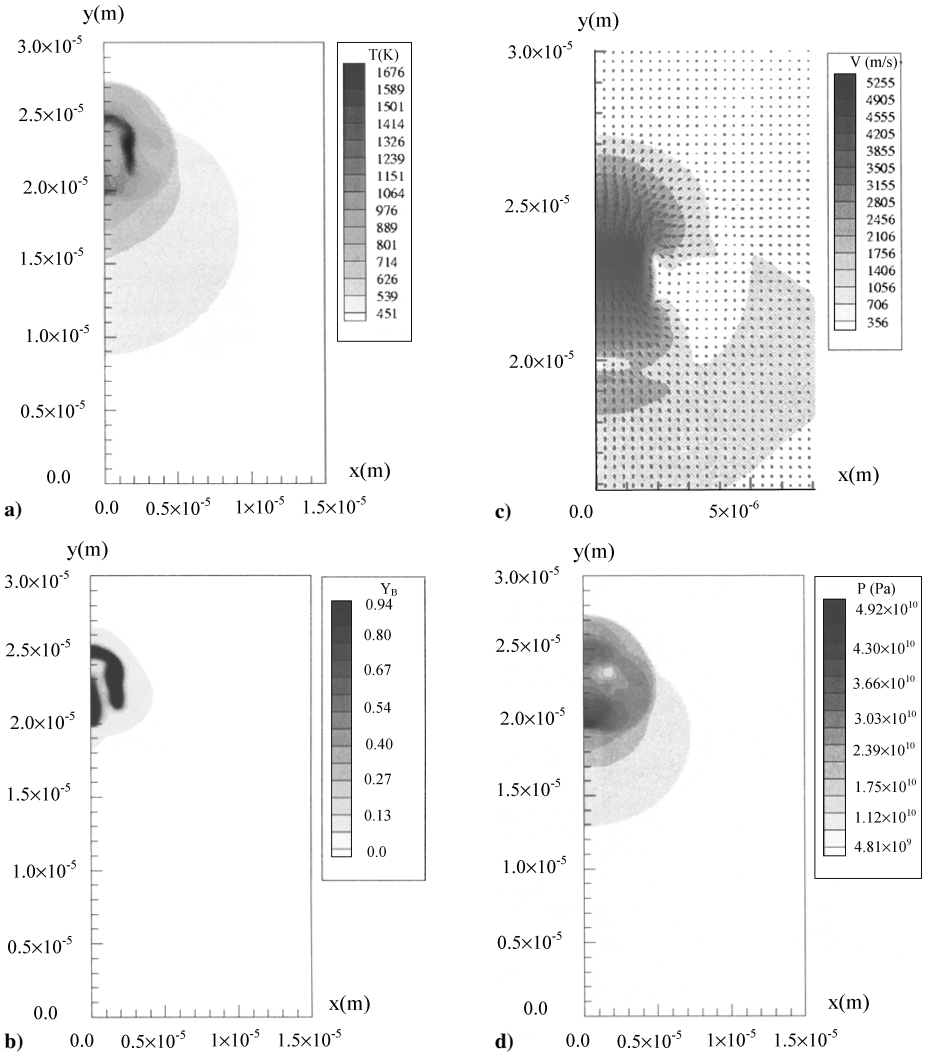

Fig. 16 Void diameter of 20 μm, U_p of 100 m/s, rise time of 10 ns, and 150×300 mesh. At instant of void collapse (24.5 ns), shown are a) temperature contour, b) species B mass fraction contour, c) velocity magnitude contour along with velocity vector, and d) pressure contour.

collapsing completely. The complete disappearance of the gaseous material is of course a numerical artifice, but the fact remains that as far as the condensed phase is concerned the gas plays a negligible thermomechanical role.

Figures 12a and 12b show the variation of maximum condensed temperature and maximum gas density plotted vs time for the different loading velocities. The rise in condensed-phase temperature at the different velocities is rather modest for the conditions simulated. The rise in the gas-phase density is rather more marked, but because the gas plays only a minor role in the void collapse process this does not appear to be of much consequence in terms of the overall energy localization mechanism.

2. Void Diameter of 20 μm

This part of the study seeks to examine the effect of void size on the void collapse and energy localization mechanisms. Figure 13 shows the evolution of the void shape for a 20-μm void, a loading velocity of 100 m/s, and a rise time of 10 ns. In the later stages of the collapse, the formation of a clear jet of material at the bottom surface of the void and the pinching of the void to form an isolated pocket is clearly seen. This behavior is qualitatively similar to that for the 10-μm-diam void. Figures 14a–14d show the contours of pressure and temperature at times of 23 and 24 ns for a loading velocity of 100 m/s. The void collapse time is larger here than for the 10-μm-diam void (for which the time of collapse was 18.4 ns). The rise in condensed-phase temperature is around 500 K, whereas the gas-phase temperature is over 1800 K, over a thin region where the void deforms the most. At the instant (24 ns) after the void pinches to form an isolated pocket, the pressures (Fig. 14c) are high in the impacted region, and the temperature (Fig. 14d) is high both in the region of impact and in the gas pocket.

Close-up view of the region near the hydrodynamic jet impact and the gas pocket is shown in Fig. 15. In this case there is a fairly large region in the condensed-phase material, where the polymer (A) has been broken down into the monomer (B). In the gas pocket there has been substantial conversion to species C (Fig. 15b) and to species D (Fig. 15c) albeit in a highly localized region. The exothermicity of the gas-phase reactions has also led to high temperatures in the gas phase (Fig. 15d).

When the void has collapsed completely at about 24.5 ns, as shown in Fig. 16, there is a strong wave associated with high temperature (Fig. 16a) and pressure (Fig. 16d) that propagates into the condensed phase originating at the location of void collapse. Associated with this are very high particle velocities (Fig. 16c) and nearly completely reacted zones with large monomer concentrations (Fig. 16b). In all of these figures, it is observed that the phenomena are much stronger for this case of larger void diameter than for the smaller diameter void. Thus, one can expect a strong effect of void size on thermomechanical coupling with chemical reactions, with larger void sizes displaying higher intensities of the phenomena. This effect might be caused by the longer collapse times of the larger voids leading to longer times over which the reactions and jet velocities can build.

Figures 17a–17d show contours of pressure and temperature at times of 14 and 15 ns for a higher loading velocity of 500 m/s. A broad and pronounced jet is formed at the lower surface, which after impact with the upper surface gives rise to high condensed-phase temperature in a region where strong compression waves form

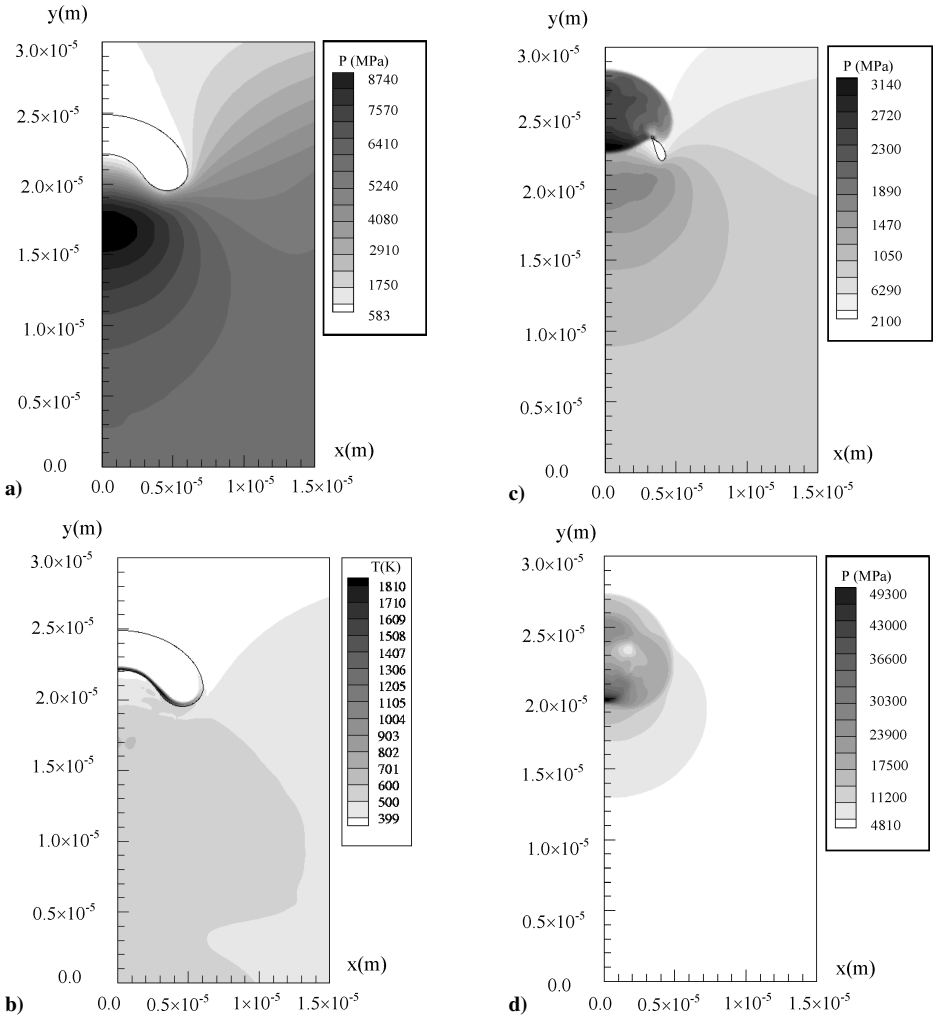

Fig. 17 Void diameter of 20 μm, U_p of 500 m/s, rise time of 10 ns, and 150×300 mesh. Shown are contours of a) pressure at 14 ns, b) temperature at 14 ns, c) pressure at 15 ns, and d) temperature at 15 ns.

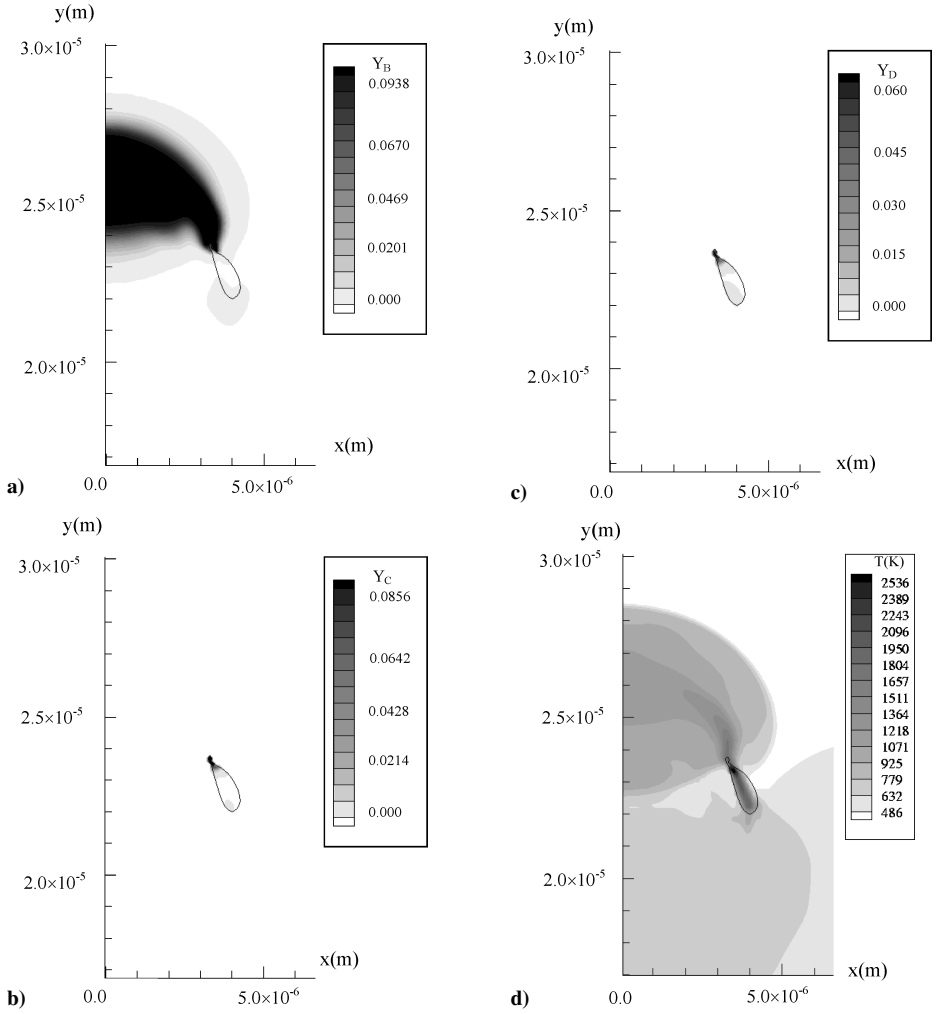

Fig. 18 Void diameter of 20 μm, U_p of 500 m/s, rise time of 10 ns, and 150×300 mesh. Close-up view of contours at 14 ns of a) species B mass fraction, b) species C mass fraction, c) species D mass fraction, and d) temperature.

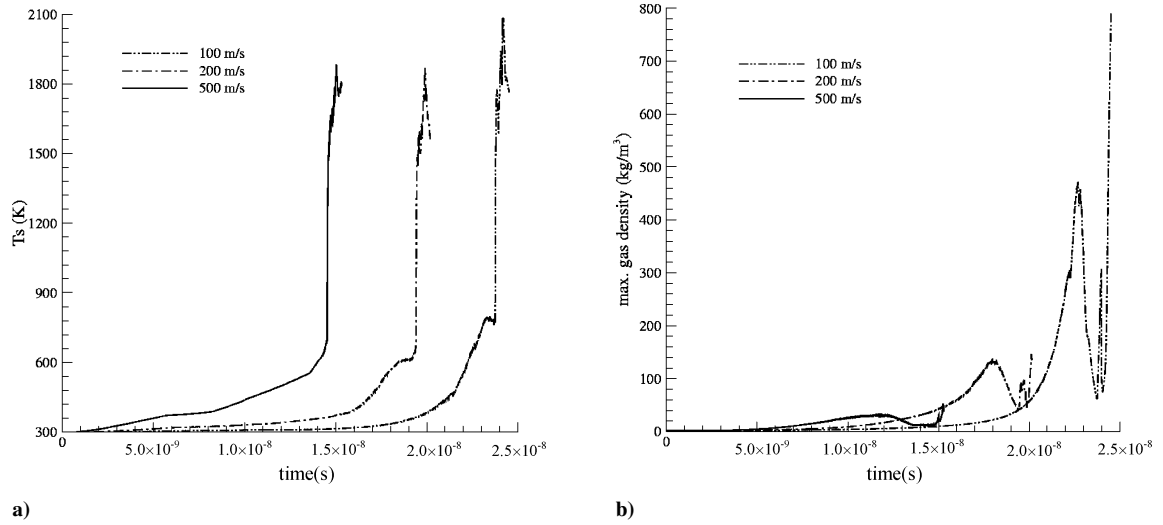

Fig. 19 Effect of loading velocities for void diameter of 20 μm, rise time of 10 ns, and 150×300 mesh. Profiles of a) maximum solid temperature vs time and b) maximum gas density vs time.

and propagate outward. Around this high condensed temperature, complete conversion of species A to species B occurs (Fig. 18a). Figure 18b–18d show that there are confined regions where further breakdown of B to form species C and D occurs. However, again there is insufficient time for these reactions to have a significant effect before the gas pocket is completely squeezed out by the collapsing condensed phase. Figure 19 shows the variation of maximum condensed-phase temperature and maximum gas density with time for the different loading velocities. The maximum temperature rise caused by viscoplastic work (values at the base of the curve before the sharp increase) is about the same for all cases. The largest temperature excursion is caused by the hydrodynamic mechanism and seems to be nearly independent of the loading velocities. The maximum temperature achieved here is around 1900 K, compared to 1300 K for the smaller void diameter of 10 μm (Fig. 12a). This reinforces the preceding conclusion that the effect of void size is

much stronger than the effect of loading velocity with regard to the intensity of localization of energy. The variation of the maximum of the gas-phase density for different impact velocities for the 20-μm void (Fig. 19b) is similar to that for the smaller 10-μm-diam void.

V. Conclusions

A numerical method has been developed and applied to study the combined gas- and solid-phase mechanics in the presence of a void, which collapses under shock loading. The chemical reactions in the condensed as well as gas phases were modeled. Calculations were performed by varying parameters that are important in the void collapse phenomenon, namely, the intensity of shock loading and the void size.

The current model allows for only one reaction to occur in the condensed phase. This is a depolymerization reaction (species A $\rightarrow$ B), which is endothermic. Following this reaction, the product B can exist in the condensed or gaseous phases. The species B, when formed in the condensed phase, is advected from the solid-void surface into the void. Thereafter, provided the gas-phase temperature is sufficiently high, species B breaks down into gas-phase products (C and D) through highly exothermic reactions. In the current system it appears that, at least for the conditions investigated, the temperatures in the condensed phase do not reach high enough values to produce much of species B. The temperature needs to be at least 800 K in the condensed phase in order for production of B to begin. Such high temperatures are only reached when the void has partially collapsed, whereby the impact of the jet of condensed material from the bottom surface of the void onto the top surface of the void leads to high enough temperatures to almost completely convert A to B in such locations. However, this does not leave enough time for the species B to accumulate in sufficient quantity in the remaining gas pockets to set off the exothermic gas-phase reactions. In fact, the effects of the gas–solid coupling in the void collapse problems studied in this paper were modest. This shortcoming of the model was not foreseen prior to the simulations.

Under the model used, the effects of the void size were far more significant than those of the loading intensity on energy localization. For a given size of void, loading intensity appears not to influence the energy localization significantly because the void collapse time scales inversely as the loading strength. Therefore for higher loading strengths the void collapses rapidly, and the events that contribute to energy localization, such as the formation of a hydrodynamic jet, are not able to build for sufficiently long durations. On the other hand, for larger voids and given loading intensity the void collapse time is longer. Hence the buildup of energy localizing phenomena can "cook" for longer times.

This work brings to light an important aspect of modeling of reactive micromechanics of void collapse. In most cases, the present simulations show that the high temperatures that could lead to the conversion of polymer HMX (species A) to its monomer form (species B) and the subsequent breakdown into gaseous reactants occur when the void completely collapses. Thus, prior to collapse the highly exothermic gas-phase reactions are limited in the void. The conventional picture of a thermal runaway caused by the thermal feedback from the gas phase caused by reactions in the gas does not seem to occur for micron-sized voids studied here with the reaction model used in this work. For sufficiently strong loading it is found that once the void collapses a large region of breakdown to yield the monomer B occurs. This region is coincident with very high temperatures and pressures. In this region the subsequent reaction steps leading to formation of C and D species and the accompanying large heat release could occur if these reactions occurred in the mixture of phases likely to be present at such a location. At the extremely high pressures and temperatures present it is difficult to characterize the state and properties of the material present, and there is little guidance that can be obtained from empirical data. Thus, further theoretical and experimental investigation is necessary to clarify the thermomechanical coupling during void collapse when chemical reactions are initiated.

Acknowledgments

This work was performed with support from the Computational Mechanics Branch, Air Force Research Laboratory/MNAC, Eglin, Florida (Project Manager Joel Stewart) and Air Force Office of Scientific Research Computational Mathematics Division (Program Manager: Fariba Fahroo).

References

[1]Margolis, S. B., Williams, F. A., and Armstrong, R. C., "Influences of Two-Phase Flow in the Deflagration of Homogeneous Solids," *Combustion and Flame,* Vol. 67, No. 3, 1987, pp. 249–258.

[2]Boggs, T. L., Price, C. F., Zurn, D. E., Derr, R. L., and Dibble, E. J., "The Self-Deflagration of Cyclotetramethylenetetranitramine (HMX)," AIAA Paper 77-857, July 1977.

[3]Kang, J., Butler, P. B., and Baer, M. R., "A Thermomechanical Analysis of Hot Spot Formation in Condensed-Phase, Energetic Materials," *Combustion and Flame*, Vol. 89, No. 2, 1992, pp. 117–139.

[4]Starkenberg, J., "Ignition of Solid High Explosive by the Rapid Compression of an Adjacent Gas Layer," *Proceedings of the 7th International Symposium on Detonation*, Naval Surface Weapons Center, White Oak, MD, 1981, pp. 3–16.

[5]Conley, P. A., "Eulerian Hydrocode Analysis of Reactive Micromechanics in the Shock Initiation of Heterogeneous Energetic Material," Ph.D. Dissertation, Dept. of Mechanical Engineering, Univ. of California, San Diego, 1999.

[6]Tran, L., and Udaykumar, H. S., "Simulation of Void Collapse in an Energetic Material, Part 1: Inert Case," *Journal of Propulsion and Power*, Vol. 22, No. 5, 2006, pp. 947–958.

[7]Conley, P. A., and Benson, D. J., "An Estimate of Solid Viscosity in HMX," *Proceedings of the 11th International Symposium on Detonation*, Office of Naval Research, Silver Spring, MD, 1998, pp. 272–289.

[8]Mitani, T., and Williams, F. A., Sandia National Lab., Rept. SAND86-8230, Livermore, CA, 1986.

[9]Lengelle, G., "Thermal Degradation Kinetics and Surface Pyrolysis of Vinyl Polymers," *AIAA Journal*, Vol. 8, No. 11, 1970, pp. 1989–1996.

[10]Peters, N., and Kee, R. J., "The Computation of Stretched Laminar Methane-Air Diffusion Flames Using a Reduced Four-Step Mechanism," *Combustion and Flame*, Vol. 68, No. 1, 1987, pp. 17–29.

[11]Peters, N., "Reduced Kinetic Mechanisms for Applications in Combustion Systems," *Fundamental Methods in Hydrodynamics*, Springer-Verlag, New York, 1993.

[12]Bonnett, D. L., and Butler, P. B., "Hot-Spot Ignition of Condensed Phase Energetic Materials," *Journal of Propulsion and Power*, Vol. 12, No. 4, 1996, pp. 680–690.

[13]McGuire, R. R., and Tarver, C. M., "Chemical Decomposition Models for the Thermal Explosion of Confined HMX, TATB, RDX, and TNT Explosives," *Proceedings of the 7th International Symposium on Detonation*, Naval Surface Weapons Center, Annapolis, MD, 1981, pp. 56–75.

[14]Tran, L., and Udaykumar, H. S., "A Particle-Level-Set-Based Sharp Interface Cartesian Grid Method for Impact, Penetration, and Void Collapse," *Journal of Computational Physics*, Vol. 193, No. 2, 2004, pp. 469–510.

[15]Li, S. C., Williams, F. A., and Margolis, S. B., "Effects of Two-Phase Flow in a Model for Nitramine Deflagration," *Combustion and Flame,* Vol. 80, No. 3–4, 1990, pp. 329–349.

[16]Strang, G., "On the Construction and Comparison of Difference Schemes," *SIAM Journal on Numerical Analysis*, Vol. 5, No. 3, 1968, pp. 506–517.

[17]LeVeque, R. J., and Yee, H. C., "A Study of Numerical Methods for Hyperbolic Conservation Laws with Stiff Source Terms," *Journal of Computational Physics*, Vol. 86, No. 1, 1990, pp. 187–210.